Cruise Slotted Wing Design with Natural Laminar Flow for Transonic Commercial Transport Aircraft

Brett R. Hiller[1], Richard L. Campbell[2], and Michelle N. Banchy[3]
NASA Langley Research Center, Hampton, VA, 23681

The present computational study investigates the aerodynamic design and analysis of cruise slotted wings with natural laminar flow for transonic commercial transport aircraft. The cruise slotted wing is a multielement wing concept that features an intermediate slot to achieve greater aft loading relative to supercritical wings for the potential benefit of reduced shock strength and pressure drag. Transonic near-cruise, off-design assessments have also shown improved drag rise characteristics due to the ability of the slot to mitigate boundary layer separation on the aft flap component. However, due to the decreased Reynolds number of the flap and increase in wetted area, the cruise slotted wing has historically incurred a skin-friction drag penalty relative to conventional supercritical wings. To offset this penalty, a cruise slotted wing with the forward main element and aft flap element shaped to achieve natural laminar flow is desired. Toward this effort, a knowledge-based aerodynamic design method, CDISC, has been leveraged to design a partial-span cruise slotted wing with natural laminar flow for a Mach-0.8 variant of the Common Research Model. Drag comparisons are provided using the USM3D-ME flow solver at cruise and near-cruise, off-design conditions relative to both fully turbulent and natural laminar flow conventional wing designs. Results at cruise show that pairing natural laminar flow design principles with the slotted wing architecture enables a 1.5 drag count reduction in cruise drag compared to conventional laminar flow wings with improved off-design performance due to the mitigation of shock-induced boundary layer separation.

Nomenclature

Acronyms

AATT	=	Advanced Air Transport Technology
AAVP	=	Advanced Air Vehicles Program
ALE	=	Align Leading Edge
ALMA	=	Aft Laminar Multielement Airfoil
BLSTA3D	=	Boundary Layer code for Stability Analysis 3D
CATNLF	=	Crossflow Attenuated Natural Laminar Flow
CDISC	=	Constrained Direct Iterative Surface Curvature
CF	=	Crossflow
CRM-M8	=	Mach-0.8 variant of the Common Research Model
CSW	=	Cruise Slotted Wing
LASTRAC	=	Langley Stability and Transition Analysis Code
LE	=	Leading Edge
NASA	=	National Aeronautics and Space Administration
NF	=	N-Factor
NLF	=	Natural Laminar Flow
TE	=	Trailing Edge
TS	=	Tollmien-Schlichting
USM3D-ME	=	Unstructured Mesh 3D, Navier-Stokes Mixed-element flow solver

[1]Research Aerospace Engineer, NASA Langley Research Center, Configuration Aerodynamics Branch, AIAA Member.
[2]Senior Research Engineer, NASA Langley Research Center, Configuration Aerodynamics Branch, AIAA Associate Fellow.
[3]Research Aerospace Engineer, NASA Langley Research Center, Configuration Aerodynamics Branch, AIAA Senior Member.

Symbols

b_{ref}	=	Configuration reference semispan, inch
c	=	Local component chord, inch
c_d	=	Sectional drag coefficient, nondimensional
C_D	=	Configuration drag coefficient, nondimensional
$c_{d,f}$	=	Sectional skin-friction drag coefficient, nondimensional
$c_{d,p}$	=	Sectional pressure drag coefficient, nondimensional
$C_{D,p}$	=	Configuration pressure drag coefficient, nondimensional
$C_{D,v}$	=	Configuration viscous drag coefficient, nondimensional
C_L	=	Configuration lift coefficient, nondimensional
c_l	=	Sectional lift coefficient, nondimensional
C_m	=	Configuration pitching moment coefficient, nondimensional
c_m	=	Sectional pitching moment coefficient, nondimensional
C_p	=	Pressure coefficient, nondimensional
c_{ref}	=	Configuration reference chord, inch
g_e	=	Slot exit gap, nondimensionalized by total local chord
g_i	=	Slot inlet gap, nondimensionalized by total local chord
M_∞	=	Freestream Mach number, nondimensional
NF	=	N-factor, nondimensional
NF^*	=	Critical N-factor, nondimensional
o_F	=	Flap overhang, nondimensionalized by total local chord
$(r/c)_{LE}$	=	Leading-edge radius, nondimensionalized by total local chord
Re_c	=	Reynolds number based on local chord, nondimensional
Re_{cref}	=	Reynolds number based on reference chord, nondimensional
S_{ref}	=	Reference area, square inch
$(t/c)_{max}$	=	Maximum airfoil thickness-to-chord ratio, nondimensional
x/c	=	x-location, nondimensionalized by total local chord
z/c	=	z-location, nondimensionalized by total local chord
α	=	Angle of attack, degree
δ	=	Deflection, degree
η	=	Semispan location, nondimensional (y/b)
γ	=	Slot inlet-to-exit gap ratio (slot ratio), nondimensional
λ	=	Midchord wing sweep, degree
ϕ	=	Twist, degree

I. Introduction

THE NASA Advanced Air Transport Technology (AATT) Project within the Advanced Air Vehicles Program (AAVP) seeks to develop next-generation technologies for fixed-wing, subsonic transports that can enable revolutionary improvements in aerodynamic efficiency. One such technology includes the Cruise Slotted Wing (CSW), which is a multielement wing concept with a forward main element and an aft flap element, separated by an intermediate slot. The purpose of the slot is to redirect airflow from the main element lower surface over the upper surface of the aft flap element, creating a "dumping velocity" at the main element trailing edge. In doing so, the flow over the airfoil upper surface is capable of undergoing only a partial pressure recovery over the main element with the off-body wake and aft flap element supporting the remaining pressure recovery to freestream conditions. Previous cruise slotted airfoil design studies demonstrated the ability of the technology to enable greater aft loading without flow separation compared to supercritical airfoils at transonic cruise conditions, in addition to a delay in drag divergence Mach number [1].

One of the key findings in this previous study was that the historically noted skin-friction drag penalty associated with cruise slotted wings could be attributed to the formation of a new boundary layer on the aft flap, which has a decreased chord Reynolds number and increased skin-friction drag relative to a supercritical airfoil over the same chordwise extent. To mitigate this penalty, the Aft Laminar Multielement Airfoil (ALMA) concept was proposed and features a flap element that is shaped to support Natural Laminar Flow (NLF) over 70% of its upper and lower surfaces [1]. A subsequent study by the authors demonstrated the design of a partial-span, cruise slotted wing using the ALMA concept for a Mach-0.8 variant of the Common Research Model (CRM-M8) [2]. At Mach 0.8, the concept was successful in offsetting the skin-friction drag penalty, compared to a supercritical wing design, while retaining favorable drag rise characteristics. The current paper extends the assessment of NLF design applied to the cruise slotted wing architecture as a potential drag-saving technology for next-generation, single-aisle commercial transports. A knowledge-based aerodynamic design method, Constrained Direct Iterative Surface Curvature (CDISC), is used to design a partial-span cruise slotted wing for the CRM-M8 with NLF over not only both surfaces on the outboard slotted wing flap, but also on the upper surface of the inboard conventional wing section and the upper surface of the outboard slotted wing main element. Additionally, fully turbulent and NLF conventional wing designs are developed using CDISC for relative performance comparisons. The objective of the study is to determine whether an NLF CSW can offer comparable drag savings to conventional NLF wing designs with the added benefit of a delay in the drag divergence Mach number. Toward this objective, the CDISC aerodynamic design code is coupled to the NASA Unstructured Mesh 3D, Navier-Stokes Mixed-element (USM3D-ME) flow solver to quantify the cruise drag differences between the configurations, in addition to near-cruise performance assessments using drag polar and drag rise simulations.

II. Design Approach

A. Computational Tools

The design and analysis process used in this work is depicted in Fig. 1 and includes a flow solver, a design module, and boundary layer stability analysis and prediction software. The design loop couples the CDISC aerodynamic design module with the NASA USM3D-ME flow solver to simultaneously converge the flow solution and wing design [3, 4]. The design process begins with generating a baseline solution at the lift-matched cruise condition using Reynolds-averaged Navier-Stokes (RANS) simulations from USM3D-ME. The analysis pressures and geometry are then extracted at a series of design stations along the wing semispan and passed to the CDISC design module. CDISC target pressure and geometry constraints are applied at the design station to create a new local airfoil shape that is expected to drive the analysis pressures closer to the target pressures, and a new blended surface wing geometry is then created. Auxiliary grid movement codes are used to deform the baseline grid to accommodate the new surface shape, which is then analyzed by USM3D-ME for the next design iteration. This process continues until adequate convergence is achieved between the USM3D-ME analysis and CDISC target pressures.

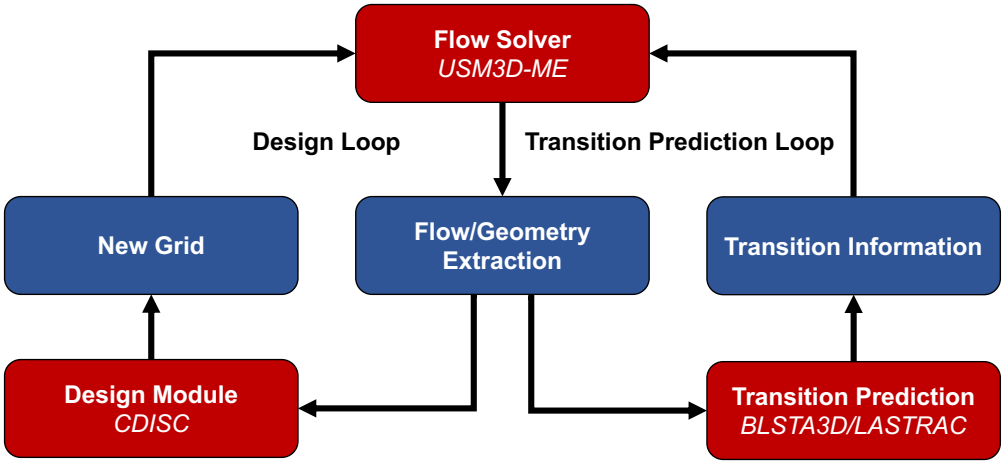

Figure 1. Flow chart of the CDISC design and analysis process.

For the NLF wing designs, laminar flow extents were determined using boundary layer stability analysis and transition prediction software consisting of two primary codes: BLSTA3D (Boundary Layer code for Stability Analysis 3D) and LASTRAC (Langley Stability and Transition Analysis Code) [5, 6]. Prior to the design process, the CDISC target pressure distributions and geometry at each design station are analyzed to estimate the chordwise transition location resulting from Crossflow (CF) and Tollmien-Schlichting (TS) boundary layer instability growth, assuming a critical N-factor of 9. The estimated transition fronts were then used as inputs within USM3D-ME to perform forced laminarization simulations, in which the turbulence production terms within the boundary layer are suppressed ahead of the transition front to model the expected regions of laminar flow. These forced laminarization simulations were used during the design process to ensure that the wing was designed in consideration of laminar boundary layer effects. Once the designs were converged with an appropriate match between the USM3D-ME analysis and CDISC target pressures, the transition prediction analysis was repeated using the design pressures to verify that the target extents of laminar flow were achieved. For off-design drag polar and drag rise analyses, fully turbulent simulations were first completed over the desired angle-of-attack and Mach number ranges, respectively. The resulting analysis pressures were then analyzed using the transition prediction software, and forced laminarization simulations were then used to assess the drag polar and drag rise performance of the NLF wing designs. This process was repeated to ensure convergence of the transition fronts, which was achieved for both wing designs in two iterations.

B. CDISC Design Method

The conventional and cruise slotted wing designs were developed using a series of CDISC aerodynamic and geometry constraints. CDISC aerodynamic constraints allow for design using typical aerodynamic variables, such as span load, sectional pitching moment coefficient, and shock strength. Additionally, geometry constraints are available to accommodate multidisciplinary concerns related to thickness, curvature, volume, and leading-edge (LE) radius. During the design process, CDISC generates target pressures on the airfoil upper surface, which are known to yield favorable performance at transonic conditions. The airfoil lower surface pressures generally remain unconstrained, allowing the geometry constraints to be enforced while satisfying the upper surface pressure targets. The primary design constraints used for slotted wing design include the aerodynamic target pressure generation constraint and the multielement geometry constraints, as shown in Fig. 2 and previously detailed in Hiller et. al [2].

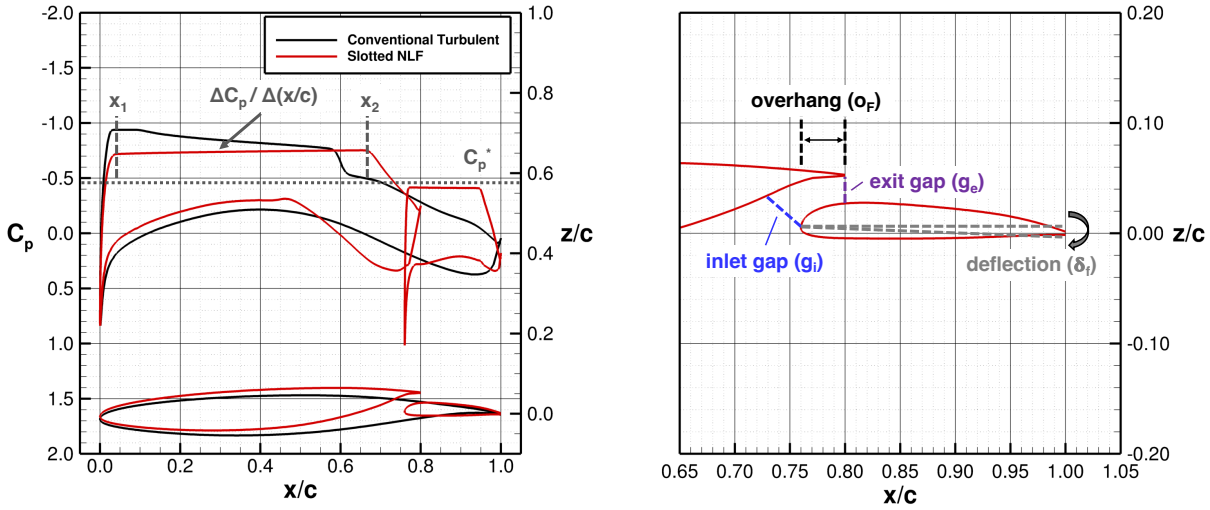

(a) Target pressure generation constraint

(b) Multielement geometry constraint

Figure 2. CDISC aerodynamic and geometry constraints for cruise slotted wing design.

The primary aerodynamic constraint used for slotted wing design is a target pressure constraint, which has been historically used in a variety of turbulent and NLF wing design applications [3], and more recently applied to multielement airfoil design [1]. The target pressure constraint, shown in Fig. 2(a), allows the user to prescribe the initial acceleration location (x_1) near the leading edge, the midchord pressure gradient ($\Delta C_p/\Delta(x/c)$), and the location for the start of the pressure recovery region (x_2) for each airfoil component. CDISC provides a set of default values for these constraint parameters based on the sectional lift and pitching moment requirements, flight condition, and design type (turbulent/NLF).

In the context of the slotted NLF wing design, the (x_1) location is set to adequately accelerate the flow near the LE such that CF boundary layer instabilities are suppressed, based on a critical N-factor of 9 at cruise conditions. The rooftop gradient is slightly favorable in order to minimize the growth of TS boundary layer instabilities. And finally, the (x_2) location was maximized to promote the largest chordwise NLF extent possible over the main element upper surface, while allowing for a smooth partial pressure recovery near the trailing edge (TE). For the flap component, the chord Reynolds number was relatively low, which permits a more gradual LE acceleration and a more adverse rooftop gradient, if desirable, compared to a conventional NLF airfoil. In this study, the (x_1) location was consistent with the flap overhang to promote attached flow through the slot, while the rooftop gradient was set to nearly zero slope to maximize flap loading. A load balancing constraint was used to maximize the flap load contribution without introducing supersonic flow, while satisfying the total sectional lift requirement. This constraint limits the supersonic flow over the flap upper surface to avoid unsteady pressure fluctuations that could lead to early transition.

The multielement geometry constraint is defined using four variables, including: flap overhang (o_F), flap deflection (δ_F), slot exit gap (g_e), and slot inlet gap (g_i), as shown in Fig. 2(b). Flap overhang is held constant during the design process and set to a value near the target chordwise location of the initial flow acceleration on the upper surface of the flap (x_1) to promote attached flow through the slot. Flap deflection is iteratively changed during the design process to help match the target LE acceleration and required sectional lift coefficient. The slot exit gap is held fixed during the design process and set based on an empirical guideline, related to the main element lower-surface boundary layer thickness at the TE, to minimize wake-boundary layer interference through the slot. Scaling the slot exit gap as a function of the lower-surface boundary layer thickness generally leads to larger suggested values near the wingtip, where the chord length reduces more rapidly than the boundary layer thickness. For this reason, the slot exit gap is held constant across the span based on best practice values near the wingtip, which provides a more conservative gap inboard to minimize wake-boundary layer interference. The slot inlet gap is implicitly defined using a slot inlet-to-exit gap ratio with CDISC best practices leveraged to maximize the main element aft loading without introducing flow separation along the main element lower surface.

III. Design Results

A. Geometry and Design Condition

The configuration chosen for the transonic cruise slotted wing assessment is a previously developed Mach-0.8 variant of the Common Research Model (CRM-M8) [2]. The research configuration was developed as a representative model of the single-aisle transonic transport class through a geometric scaling of the original CRM, in addition to unsweeping the wing for a reduced cruise Mach number using simple sweep theory. To facilitate a more efficient design exploration study, the CRM-M8 includes only the wing and fuselage components. The CRM-M8 cruise condition is Mach 0.8 with a Reynolds number based on reference chord, Re_{cref}, of 21.1 million and a cruise lift coefficient, C_L, of 0.543, as listed in Table 1 along with the geometry reference parameters.

Table 1. Geometry reference parameters and cruise condition for the CRM-M8 configuration.

Configuration	c_{ref} (in)	b_{ref} (in)	S_{ref} (in^2)	λ	M_∞	Re_{cref}	C_L
CRM-M8	165.5	694.05	107,050	25°	0.80	21.1×10^6	0.543

Figure 3 shows the baseline geometries for a conventional wing variant, as well as a partial-span cruise slotted wing variant. The baseline conventional wing geometry was used to develop both conventional turbulent and NLF wing designs using CDISC. The cruise slotted wing geometry retains an identical single-element inboard wing section to mitigate multidisciplinary concerns related to system integration, i.e., fuel tanks, landing gear, structures, etc. The slotted outboard wing section begins at a nondimensional semispan location, η, of approximately 37%. An in-house MAKESLOT code was used to create the outboard slotted wing section using the conventional turbulent wing design as the seed geometry. The baseline slotted wing features a main element with a chord length equal to 82% of the conventional wing total chord, and a flap element with an overhang (o_F) of 4% total chord and a deflection (δ_F) of 2 degrees. The baseline slot geometry has an exit gap (g_e) of 2.5% total chord based on previously published CDISC best practices to avoid interference between the main element wake and flow above the flap element. The slot inlet gap (g_i) was calculated based on a best practice slot inlet-to-exit gap ratio of 1.2 to maximize the aft loading over the main element without introducing flow separation along the lower surface toward the entrance of the slot. These slotted wing design parameters were held constant during the design process with the exception of flap deflection, which was allowed to change to accommodate the desired LE acceleration characteristics based on the prescribed target pressures.

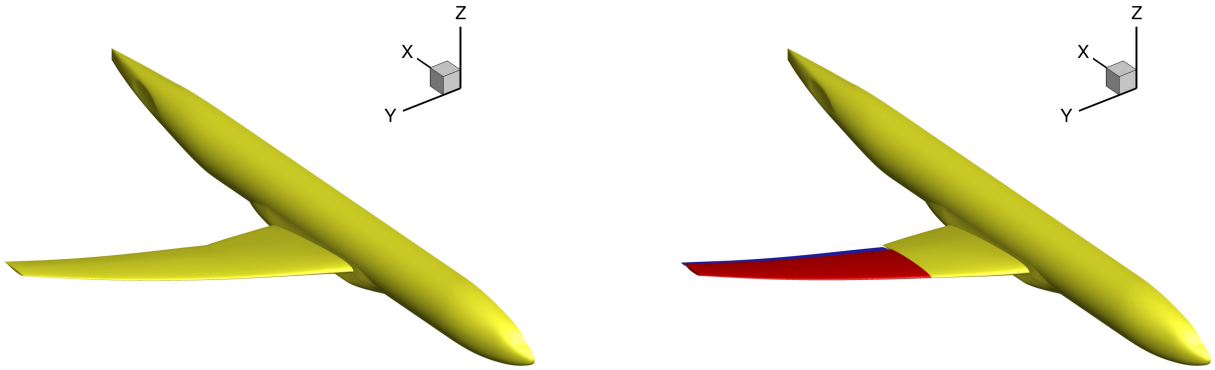

(a) Conventional wing (b) Slotted wing

Figure 3. Baseline geometry for conventional (left) and slotted (right) wing variants of the CRM-M8.

B. Design Stations

To maintain consistency between the conventional and slotted wing variants, the CDISC design process was set up using 13 design stations along the wing semispan, as shown in Fig. 4. The fully turbulent conventional wing design for the CRM-M8 was completed in a previous publication [2] and used to define the target spanwise load distribution for both NLF designs to eliminate performance differences due to changes in induced drag. The six stations denoted by dashed lines serve as reference design stations for reviewing select geometry and target pressure variations along the wing. The stations include two inboard and four outboard semispan locations, ranging from η = 0.11 to 0.95 with a decrease in local chord Reynolds number (Re_c) from 35.5 to 9.3 million, as noted in Table 2.

Table 2. Parameters for reference wing design stations.

Station	Location	η	Chord (ft)	Re_c (million)
1	Inboard	0.11	23.2	35.5
3	Inboard	0.28	17.3	26.5
6	Outboard	0.45	13.2	20.2
8	Outboard	0.61	11.0	16.8
10	Outboard	0.78	8.5	13.0
12	Outboard	0.95	6.1	9.3

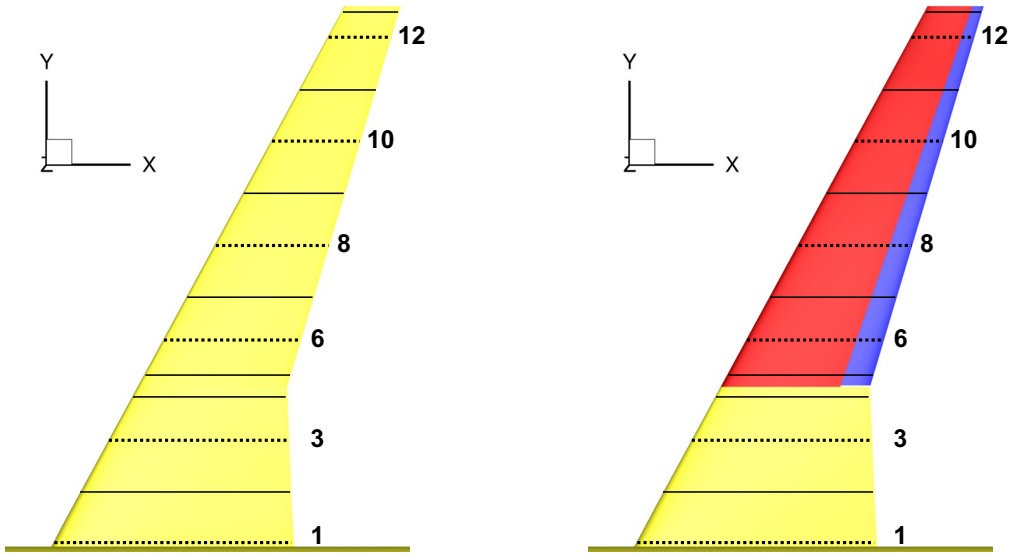

(a) Conventional wing

(b) Slotted wing

Figure 4. Baseline geometry for conventional (left) and slotted (right) wing variants of the CRM-M8.

C. Wing Designs

The fully turbulent conventional wing design for the CRM-M8 was previously documented in Hiller et al. and served as a reference design for the current study [2]. The primary objective of this research was to determine the relative performance between a cruise slotted NLF wing and a conventional NLF wing at both cruise and near-cruise, off-design conditions. These wing designs were developed by coupling the CDISC design code with the USM3D-ME flow solver, as detailed in Section II, and designed for a cruise condition of M = 0.8, Re_{cref} = 21.1 million, and C_L = 0.543. For both NLF wing designs, the span loading of the conventional turbulent wing design was used as the target span load to mitigate cruise drag differences due to induced drag.

In terms of aerodynamic constraints, the conventional NLF wing design used the CDISC target pressure generation constraint for laminar airfoil design to obtain NLF over the wing upper surface. This is a common practical assumption in consideration of lower surface gaps or steps that might be introduced due to high-lift devices or access panels. In the case of the slotted NLF wing, the common single-element inboard section was designed for NLF on the wing upper surface to maintain consistency with the conventional NLF wing. For the outboard slotted wing section, the slotted airfoil constraints described in Section II.B were used to target NLF over the forward main element upper surface, as well as both surfaces of the aft flap element. For this initial aerodynamic assessment, it is assumed that the flap element would be free of steps or gaps that could lead to early transition, and slot bracket hardware is not modeled to reduce design complexity. Inclusion of slot brackets would ultimately lead to localized turbulent wedges over the surface that is expected to reduce the potential NLF flap drag benefit. If a significant drag reduction were identified, future studies could include modeling of flap brackets, as well as accounting for any structural weight penalties or aircraft resizing implications. The goal of the present study is to quantify the best-case cruise drag benefit to determine whether more detailed design exploration studies are warranted for consideration of the NLF cruise slotted wing as a drag-saving technology on next-generation aircraft.

The final USM3D-ME sectional pressure distributions and geometries for the conventional turbulent, conventional NLF, and slotted NLF wing designs are illustrated in Fig. 5. Results are provided for two inboard stations (1 and 3) to confirm consistency between the two designs over the common single-element section and for two outboard designs stations (8 and 10) to highlight the cruise slotted wing design differences. The target and analysis pressures were in close agreement for each wing design, so only the analysis pressures are shown for brevity. The airfoil geometries have a TE anchored to z/c = 0 to highlight the potential twist differences between the conventional and slotted wing designs. Over the common inboard section, similar pressures are achieved for the conventional NLF and slotted NLF wing designs due to the use of identical design constraints. At station 1 near the wing root, NLF is not specifically targeted as a turbulent wedge often grows near the root leading edge, and achieving the required LE acceleration to

suppress CF growth is more challenging due to structural constraints, such as airfoil thickness and leading-edge radius. Minor differences are observed for both NLF wing designs relative to the conventional turbulent wing design due to the impact of twist smoothing and the design of further outboard stations for NLF. Station 3 shows a typical NLF pressure distribution for the conventional and slotted NLF wing designs. At the leading-edge, there is a rapid flow acceleration followed by an abrupt flattening of the upper surface C_p to control transition due to CF. A slightly favorable C_p gradient is then introduced to mitigate the growth of TS instabilities. This C_p gradient is sustained back to approximately x/c = 0.65, where the terminating shock is located to provide a smooth pressure recovery near the TE without flow separation. The end of this region signifies the transition from laminar to turbulent flow over the wing upper surface. The NLF airfoils show minor reductions in both twist and leading-edge radius relative to the conventional turbulent wing design.

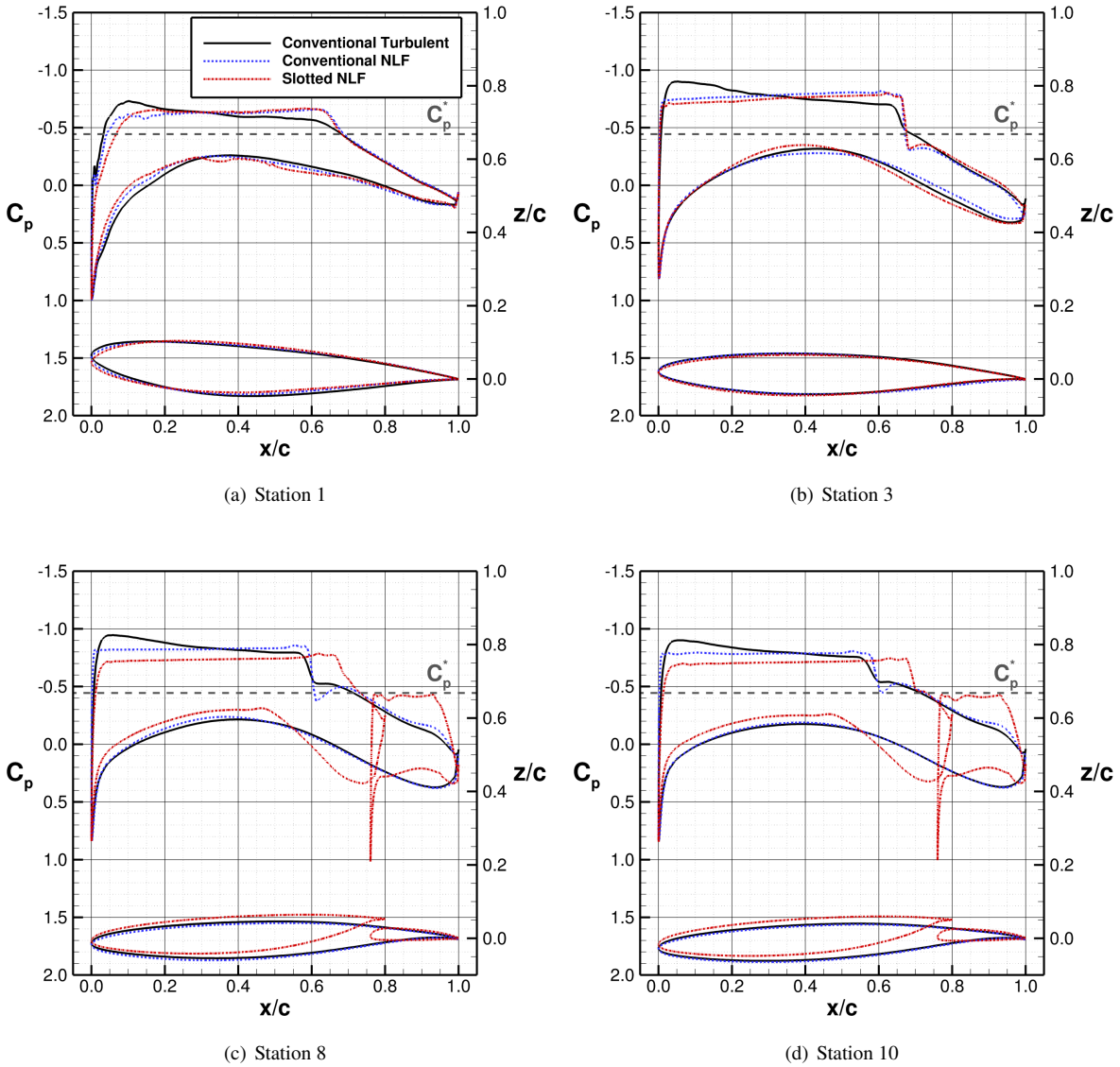

(a) Station 1

(b) Station 3

(c) Station 8

(d) Station 10

Figure 5. Sectional pressures and geometry at select design stations for the CRM-M8 conventional and slotted wing designs.

For the outboard design stations 8 and 10, shown in Figs. 5(c) and 5(d), similar pressures and geometry features are observed for the conventional NLF wing design. The slotted NLF wing design includes the pressures and geometry for both the main element and flap. CDISC was able to successfully design the pressures using the strategy detailed in Section II.B with close agreement to the target pressures (not shown). For the slotted airfoil sections, a load balancing constraint was used to maximize the flap loading while retaining subsonic flow to avoid shocks or unsteady flow through the slot or over the laminar flap element surfaces. Furthermore, the slot was carefully shaped to maximize main element aft loading without introducing flow separation. As a result, a notable increase in aft loading is observed for the slotted NLF wing compared to the conventional wing designs. By increasing the aft loading, the main element sectional lift requirement is reduced. Additionally, because the main element upper surface only needs to undergo a partial pressure recovery nears its TE, the main element shock position could be shifted aft by approximately 10% compared to the conventional wing designs. The expected impact on drag is a reduction in transonic wave drag through weakening of the shock.

In terms of natural laminar flow, the main element upper surface pressure distribution qualitatively resembles the features of a conventional NLF wing with a rapid LE acceleration followed by an abrupt shift to a slightly favorable C_p gradient back to the terminating shock near x/c = 0.7. By shifting the terminating shock location aft, the main element upper surface achieves approximately a 10% increase in laminar flow compared to a conventional NLF wing. Similar pressure features are observed for the flap, which helps achieve laminar flow over approximately 70% of the flap upper surface. Furthermore, due to the relatively low chord Reynolds number of the flap, laminar flow is also attained over approximately 70% of the flap lower surface using a curvature constraint to limit the adverse pressure gradient and mitigate transition due to TS. Ultimately, the slotted NLF wing helps to achieve greater extents of laminar flow compared to a conventional NLF wing by providing a more gradual upper surface pressure recovery and by reshaping the flap for laminar flow over both surfaces. This benefit should result in reduced skin-friction drag provided that the design can offset the drag penalty associated with multielement wings.

The variation in sectional aerodynamic and geometry constraints for the conventional turbulent, conventional NLF, and slotted NLF wing designs are illustrated versus nondimensional semispan (η = y/b) in Fig. 6. The sectional lift (c_l) distribution shows that both the conventional NLF and slotted NLF wing designs were able to closely match the target span load from the conventional turbulent wing design. The sectional pitching moment (c_m) distribution shows a decrease over the outboard section for both the conventional NLF and slotted NLF wing designs compared to the conventional turbulent wing design. For the conventional NLF wing, this decrease in pitching moment results from a mild increase in aft loading due to the favorable C_p gradient over the upper surface, which helps to suppress TS growth at the expense of a slightly stronger shock. For the slotted NLF wing, there is a notable decrease in pitching moment by approximately 50% due to achieving greater aft loading.

In terms of geometry constraints, the maximum airfoil thickness ($(t/c)_{max}$) was held constant along the span between the three wing designs, and the leading-edge radius ($(r/c)_{LE}$) was limited to approximately a 10% variation between the designs. This was done to limit system integration and off-design performance concerns between the three configurations. Finally, the twist (ϕ) distribution shows the conventional turbulent and NLF wing designs in close agreement, despite notable changes to the conventional NLF wing upper surface pressure distribution to facilitate laminar flow. In contrast, a twist discrepancy is observed for the slotted NLF wing compared to both conventional wing designs. In the region of the planform break, there is a notable change in twist as the wing transitions from a single-element to multielement airfoil section. The slotted wing outboard twist (measured relative to the flap TE) is slightly greater compared to the conventional wings due to the difference in aft loading achieved. As a result, this can lead to a geometry discontinuity near the planform break. An additional Align Leading Edge (ALE) constraint was used for the slotted wing design to blend the wing geometry and twist changes across the planform break. The use of twist smoothing causes the inboard twist distribution to be slightly altered compared to the conventional wings. Overall, CDISC was successful in achieving the slotted wing target pressures over the outboard wing, while meeting imposed geometry constraints for a practical wing design with reduced system integration concerns.

For the conventional NLF and slotted NLF wing designs, transition prediction software was utilized before the design process to ensure that the wing target pressures would achieve the expected extents of laminar flow. This helped to estimate the transition fronts over the wing upper surface and both surfaces of the flap for the slotted wing design. These transition fronts were then used to perform USM3D-ME forced laminarization simulations during the design process to ensure that the airfoil components were reshaped in consideration of laminar boundary layer effects. The resulting design pressures were then analyzed with the transition prediction software to ensure that the target extents of laminar flow were attained. The following section summarizes the cruise transition predictions for both the conventional NLF and slotted NLF wing designs.

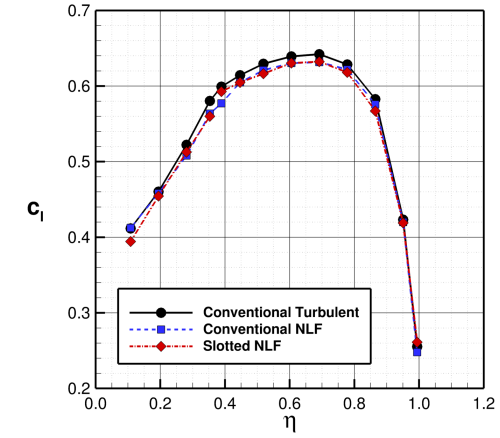

(a) Lift coefficient

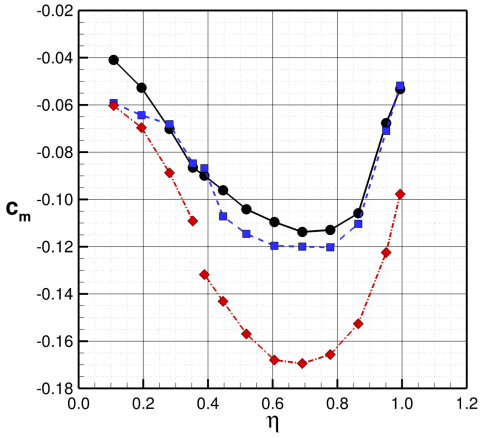

(b) Pitching moment coefficient

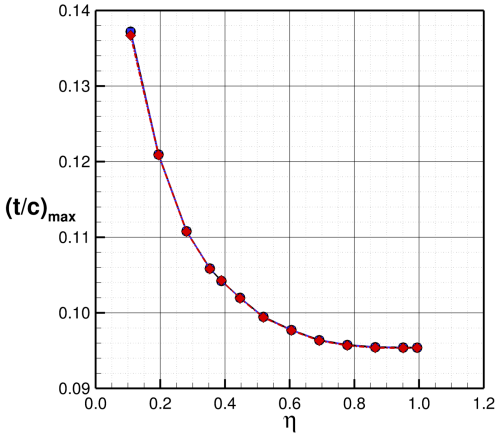

(c) Thickness

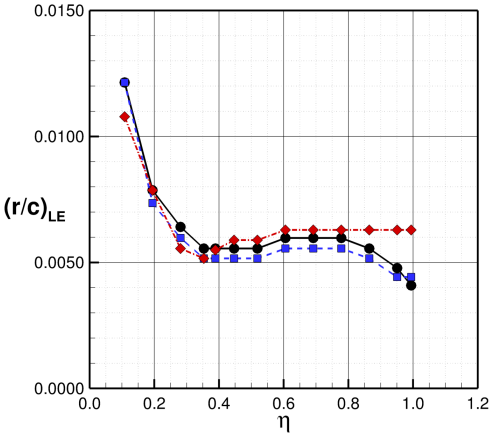

(d) Leading-edge radius

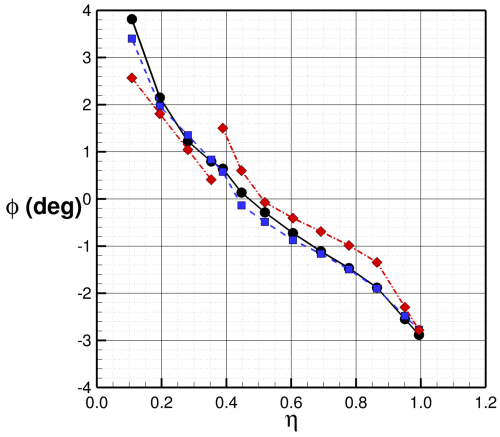

(e) Twist

Figure 6. Spanwise distributions of aerodynamic and geometry constraints for the CRM-M8 conventional and slotted wing designs.

D. Natural Laminar Flow Assessment

A boundary layer stability analysis was performed for the conventional NLF and slotted NLF wing designs at cruise conditions to confirm the estimated extents of laminar flow were achieved. The geometry and design pressures were evaluated using the boundary layer profile solver, BLSTA3D, and the stability analysis code, LASTRAC, which are described in Section II.A. Figure 7 shows the predicted laminar flow extents, CF N-factor growth, and TS N-factor growth at inboard design station 3 for both wing designs. Given that the inboard section is common to both wing designs, similar laminar flow extents are achieved. The CF analysis shows that the pressure alterations near the LE were successful in damping CF instabilities below NF^* with sufficient margin. The TS analysis shows that the favorable rooftop gradient was successful in limiting the growth of TS instabilities up to the aft shock location. As a result, laminar flow was achieved over approximately 60% of the wing upper surface area for both designs.

Figure 8 highlights the predicted laminar flow extents, CF N-factor growth, and TS N-factor growth at outboard design station 8 for both wing designs. In the slotted wing case, transition predictions are included for the main element upper surface, flap upper surface, and flap lower surface. At the Mach 0.8, Re_{cref} = 21.1 million cruise condition, the conventional NLF wing successfully dampens the growth of CF and TS instabilities using the CDISC target pressure generation constraint best practices for NLF design. For the slotted wing, the main element upper surface pressure distribution, shown previously in Fig. 5, was characterized with a slightly more gradual leading-edge acceleration compared to the conventional NLF wing. This was done based on limitations to the LE acceleration that could be achieved near the planform break due to the airfoil geometry transition. As a result, this leads to greater CF growth over the main element upper surface but remains well below NF^*. For the flap upper and lower surface, CF growth is reduced due to the relatively low chord Reynolds number of the flap and concerns for transition due to CF instabilities are limited. The TS growth over the main element upper surface remains comparable to that of the conventional NLF wing but approximately a 5% increase in laminar flow extent is achieved at station 8 due to the aft translation of the main element shock. Similar to CF, the growth of TS instabilities is easily suppressed over the both surfaces of the flap, and laminar flow is achieved over nearly 70% of the flap chord, up to the aft pressure recovery region.

After computing the transition location due to CF and TS at each station, a transition front was determined for the conventional NLF wing upper surface (US), as well as the upper surfaces of the inboard wing and main element and both surfaces of the flap for the slotted NLF wing. The resulting transition front predictions over the upper surfaces of the two wing designs area shown in Fig. 9. For the conventional NLF wing, laminar flow was shock-limited but achieved over approximately 53% of the wing upper surface area. The lower surface was not targeted for NLF due to the expected presence of gaps or steps, due to access panels or high-lift device integration, which would trip the flow. For the slotted NLF wing, laminar flow was also shock limited with the exception of a more forward transition in the vicinity of the planform break. This forward transition was primarily due to an inability to exactly match the target C_p gradient needed to suppress TS growth due to the use of geometry smoothing constraints for blending the two wing sections. For the outboard slotted wing section, the main element shock location was shifted aft by 10%, which helped to increase the extents of laminar flow over the wing upper surface. Additionally, laminar flow was achieved over approximately 70% of the flap element, which helped to increase the total NLF area over the upper surface from 53% with the conventional wing to 61% with the slotted wing. While not shown, reshaping the lower surface of the flap achieved laminar flow over 70% of the flap lower surface or approximately 10% of the total wing lower surface area. As a result, the slotted wing design was able to successfully increase the total NLF wing area from 27% to 35% at cruise conditions for the single-aisle CRM-M8 transport configuration. These transition front predictions were then used to facilitate USM3D-ME forced laminarization simulations to estimate the aerodynamic performance of the conventional and slotted NLF wing designs.

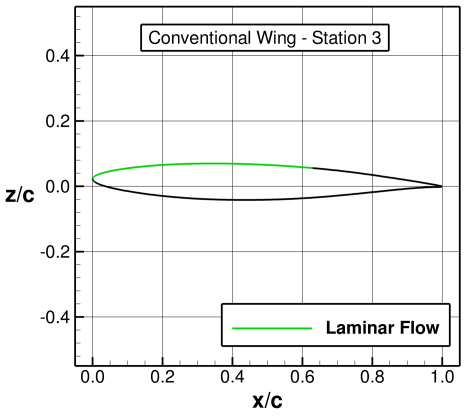

(a) Laminar flow extent - conventional NLF wing

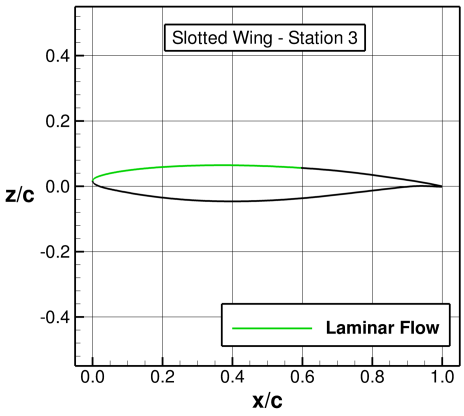

(b) Laminar flow extent - slotted NLF wing

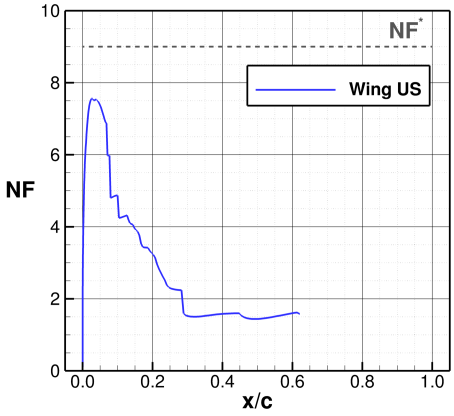

(c) CF growth - conventional NLF wing

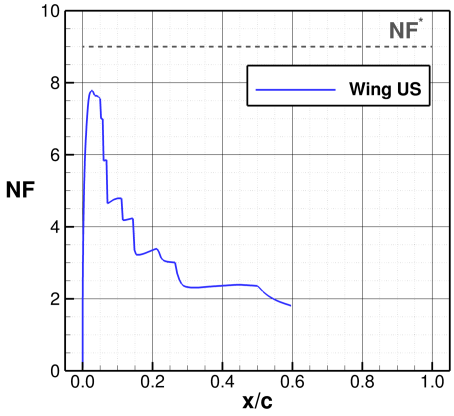

(d) CF growth - slotted NLF wing

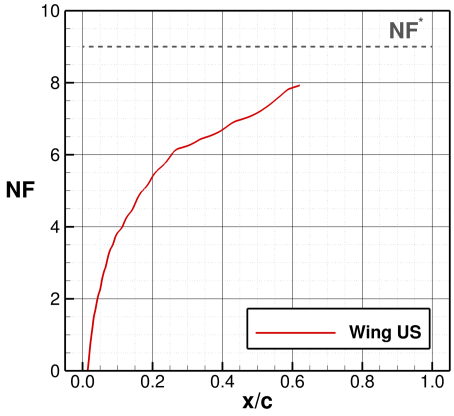

(e) TS growth - conventional NLF wing

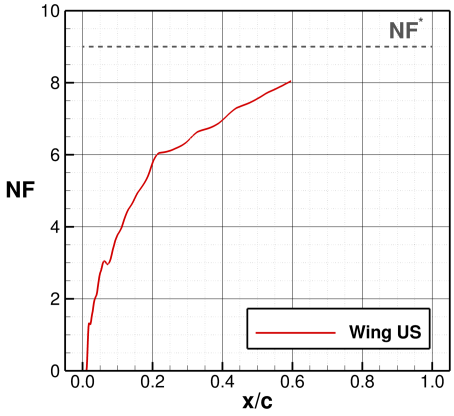

(f) TS growth - slotted NLF wing

Figure 7. Laminar flow extents, CF growth, and TS growth at design station 3 for the CRM-M8 conventional and slotted wing designs.

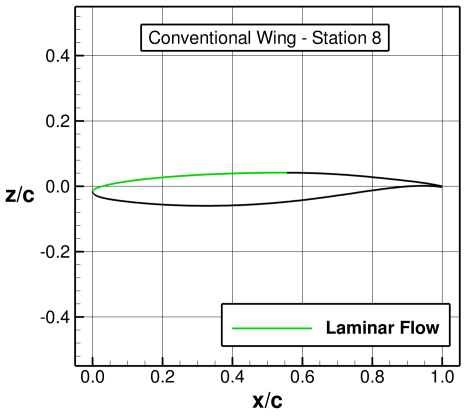

(a) Laminar flow extent - conventional NLF wing

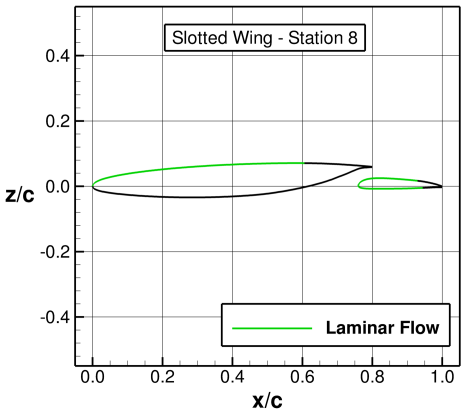

(b) Laminar flow extent - slotted NLF wing

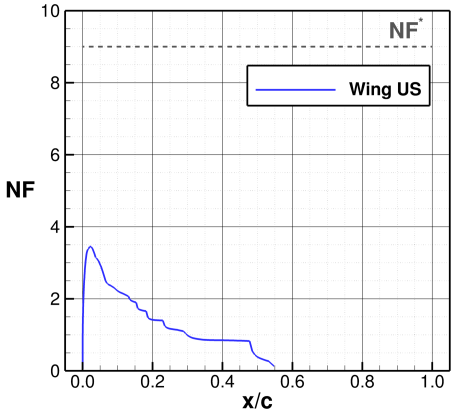

(c) CF growth - conventional NLF wing

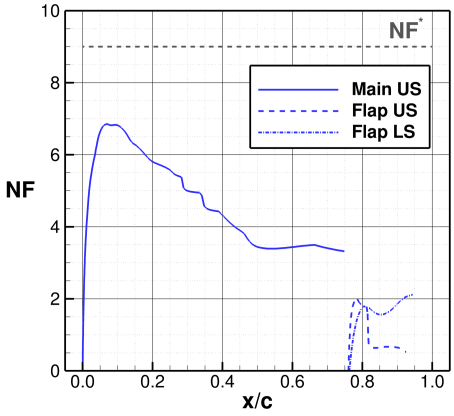

(d) CF growth - slotted NLF wing

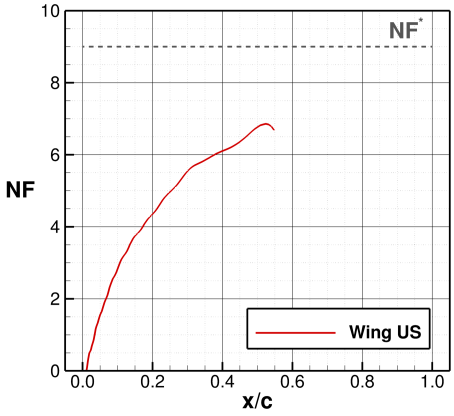

(e) TS growth - conventional NLF wing

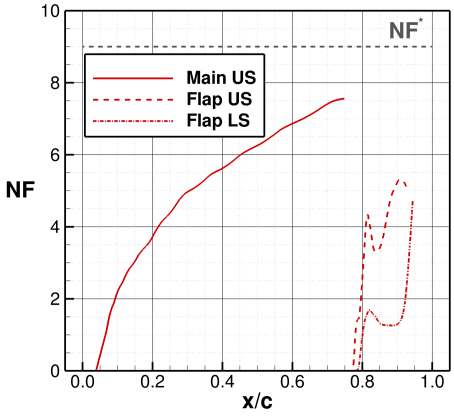

(f) TS growth - slotted NLF wing

Figure 8. Laminar flow extents, CF growth, and TS growth at design station 8 for the CRM-M8 conventional and slotted wing designs.

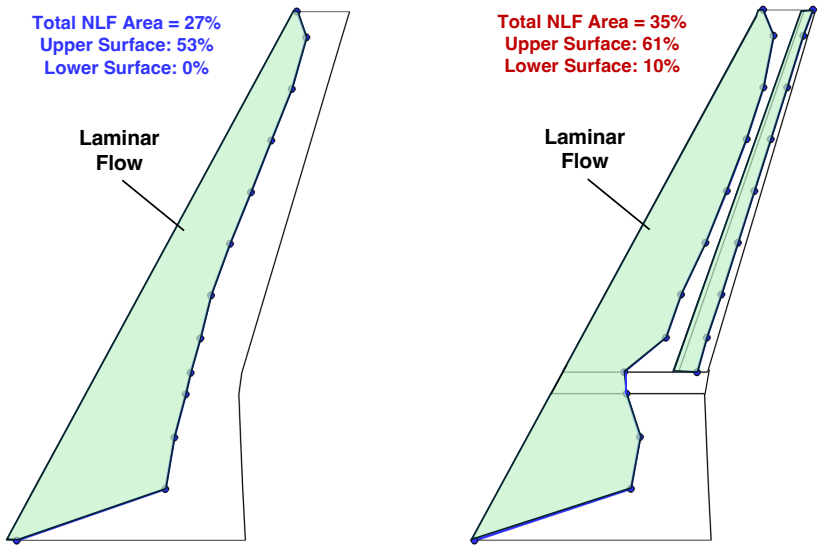

(a) Conventional wing (b) Slotted wing

Figure 9. Transition front predictions at cruise for conventional (left) and slotted (right) NLF wing variants of the CRM-M8

E. Cruise Performance

USM3D-ME forced laminarization simulations were completed for both the conventional and slotted wing designs for performance comparisons with the conventional turbulent wing, as summarized in Table 3. Fully turbulent simulations were also completed for the NLF designs to model loss of NLF as an off-design consideration. In each case, the configuration angle of attack was perturbed to match the cruise lift coefficient. The conventional NLF wing was successful in reducing the cruise drag coefficient relative to the conventional turbulent wing by 0.00184 or 18.4 drag counts (drag count, 1 ct ≡ 0.0001 of C_D). For the slotted NLF wing design, the cruise drag was further reduced by an additional 1.4-ct for a total drag reduction of 19.8-ct relative to the conventional turbulent wing. This result can be attributed to a decrease in both viscous and pressure drag due to the slotted wing benefits. In the case of loss of laminar flow, the fully turbulent drag penalty for the slotted wing is approximately 0.8-ct worse than the conventional NLF wing. This mild increase in drag for the slotted wing at fully turbulent conditions, compared to the conventional NLF wing, may be attributed to the increased skin-friction drag associated with multielement wings. The configuration pitching moment coefficient (C_m) reflects the change in aft loading between the conventional and slotted NLF wing designs. Since only a wing-body configuration was considered in the present study, the impact of trim drag was not modeled, though the pitching moment variability remains limited between the three configurations. Ultimately, the slotted NLF wing design was successful in providing a cruise drag benefit compared to a conventional turbulent wing design with a slight improvement compared to the conventional NLF wing through reductions in viscous and pressure drag.

Table 3. Total force and moment coefficient data for the CRM-M8 conventional and slotted wing designs at the cruise condition of M_∞ = 0.8, Re_{cref} = 21.1 million, and C_L = 0.543.

Model	α (deg)	C_L	C_D	$C_{D,v}$	$C_{D,p}$	C_m	L/D
Conventional Turbulent Wing	2.1	0.543	0.02382	0.00941	0.01441	0.016	22.8
Conventional NLF Wing	2.1	0.543	0.02198	0.00835	0.01363	0.006	24.7
Conventional NLF Wing (loss of NLF)	2.5	0.543	0.02446	0.00935	0.01511	0.028	22.2
Slotted NLF Wing	2.1	0.543	0.02184	0.00827	0.01357	-0.016	24.9
Slotted NLF Wing (loss of NLF)	2.5	0.543	0.02453	0.00976	0.01477	0.007	22.1

It was noted that the slotted NLF wing provided decreases in both viscous and pressure drag compared to the conventional NLF wing. A cruise drag decomposition is provided in Fig. 10 to assess the total, viscous, and pressure drag contributions of the fuselage, inboard wing, outboard wing, and trailing-edge components. The total drag contributions show that the wing design strategy was generally successful in matching the fuselage and inboard wing drag between the two designs in order to isolate total drag differences to the outboard wing design. The viscous drag savings for the conventional and slotted NLF wing designs are comparable over the common inboard sections, while the slotted wing shows a slight decrease in viscous drag over the slotted wing section. Furthermore, the pressure drag over the inboard wing section is comparable between the two designs; however, the slotted wing shows an increase in pressure drag over the outboard section compared to the conventional NLF wing. This was unexpected due to the beneficial aft translation and weakening of the main element upper surface shock. To better understand the differences in pressure drag contributions between the inboard and outboard wing sections, the pressure and skin-friction distributions at each design station were integrated to show how pressure and viscous drag change with wing semispan.

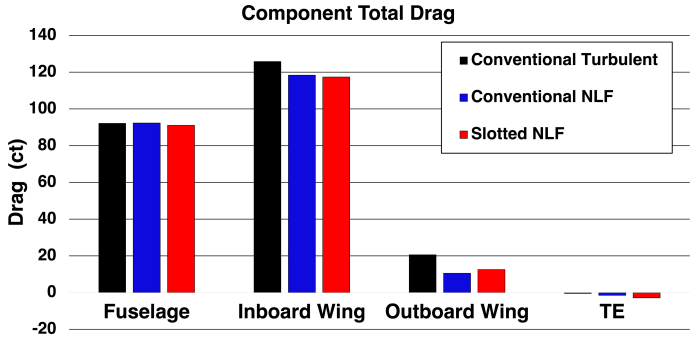

(a) Total drag

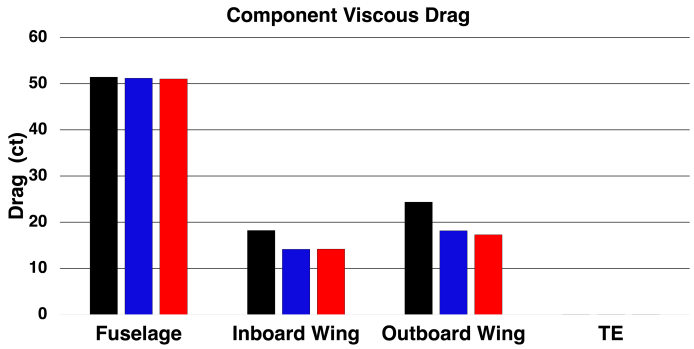

(b) Viscous drag

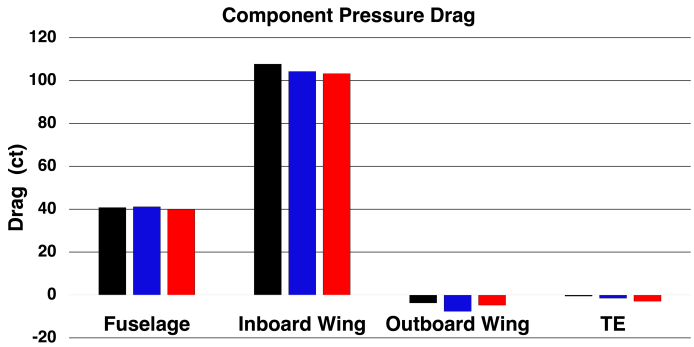

(c) Pressure drag

Figure 10. Component contributions to total, viscous, and pressure drag at cruise for the CRM-M8 conventional and slotted wing designs.

Figure 11 shows the distributions of sectional pressure and skin-friction drag versus nondimensional semispan (η) for the wing designs. For skin-friction drag, both the conventional NLF and slotted NLF wing designs show an expected, significant decrease compared to that of the conventional turbulent wing due to reshaping of the wing to promote natural laminar flow. Over the outboard slotted wing section, there is a further decrease in viscous drag for the slotted wing design due to the increased NLF surface area achieved. However, there is a slight increase in skin-friction drag near the planform break, where geometry smoothing constraints limit the achievable extents of laminar flow. For pressure drag, the slotted NLF wing was not able to achieve a significant reduction compared to the conventional wing designs despite a mild decrease in main element shock strength. Furthermore, the impact of geometry smoothing near the planform break leads to a slight increase in pressure drag. At the Mach 0.8 cruise condition, pressure drag benefits appear limited for the slotted wing architecture since the flap loading must be limited to prevent introducing unsteady supersonic flow that could lead to early transition and a trade-off increase in skin-friction drag.

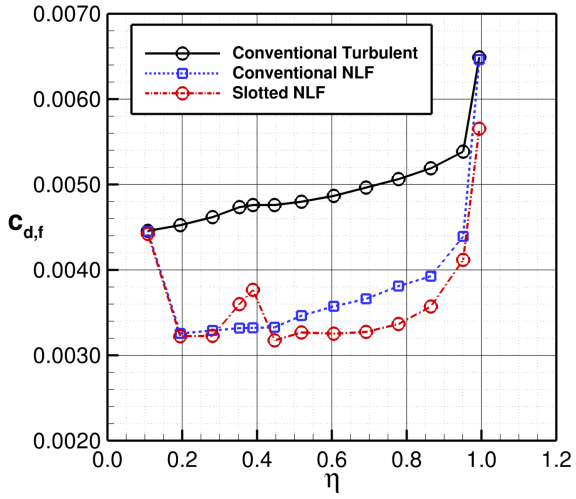

(a) Sectional skin-friction drag

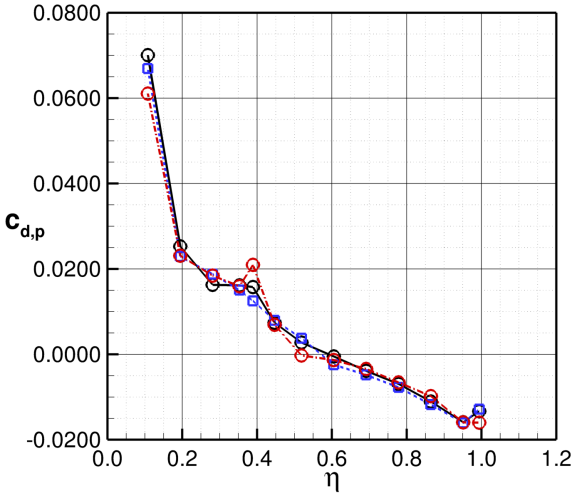

(b) Sectional pressure drag

Figure 11. Spanwise distributions of sectional skin-friction and pressure drag coefficients for the CRM-M8 conventional and slotted wing designs.

IV. Off-Design Results

In addition to evaluating the relative cruise drag performance between the conventional and slotted NLF wing designs, a near-cruise, off-design assessment was conducted using drag polar and drag rise analyses. Transition predictions were used to assess laminar flow sensitivity as a function of angle of attack and Mach number, in addition to fully turbulent analyses for loss of laminar flow considerations. A partial loss of laminar flow can be anticipated at off-design flight conditions when flow perturbations lead to early transition due to the growth of CF/TS instabilities or when exposed to contaminates, such as bugs, icing, or surface imperfections, that can lead to bypass transition. The fully turbulent loss of laminar flow simulations serve as a worst-case performance scenario for the NLF wing designs.

A. Drag Polar

Turbulent drag polar simulations were conducted at the cruise Mach number of 0.8 over an angle-of-attack range from 0° to 3.5° with 0.5° increments to sample an approximate C_L range of 0.2 to 0.7. This specific range includes the ±10% $C_{L,cruise}$ range to assess NLF sensitivity at near-cruise, as well as up to 1.3*$C_{L,cruise}$, which is considered a relevant buffet condition. Transition predictions were performed using the fully turbulent pressures to estimate regions of laminar flow through the drag polar range. USM3D-ME forced laminarization predictions were then used to simulate the predicted extents of NLF for the conventional and slotted wing designs as a function of angle of attack. The pressure distributions from the forced laminarization simulations were reassessed using transition predictions, and the simulation process was repeated until drag polar convergence was achieved.

Figure 12 shows the resulting drag polar results for each of the three wing designs. At cruise conditions, it is observed that the conventional NLF and slotted NLF wing designs maintain a drag benefit compared to the conventional turbulent wing throughout the polar range. The slotted NLF wing matches the conventional NLF wing performance at near-cruise conditions but shows a slight drag benefit at higher lift coefficient values. At lower lift coefficient values, the slotted NLF wing incurs a drag penalty relative to the conventional NLF wing. At fully turbulent, loss of laminar flow conditions, both configurations maintain a turbulent drag penalty relative to the conventional turbulent wing design at near-cruise conditions. Near the buffet condition (1.3*$C_{L,cruise}$), the slotted NLF wing showed a 15% improvement in aerodynamic efficiency (L/D) compared to the conventional turbulent wing and a 5% improvement relative to the conventional NLF wing.

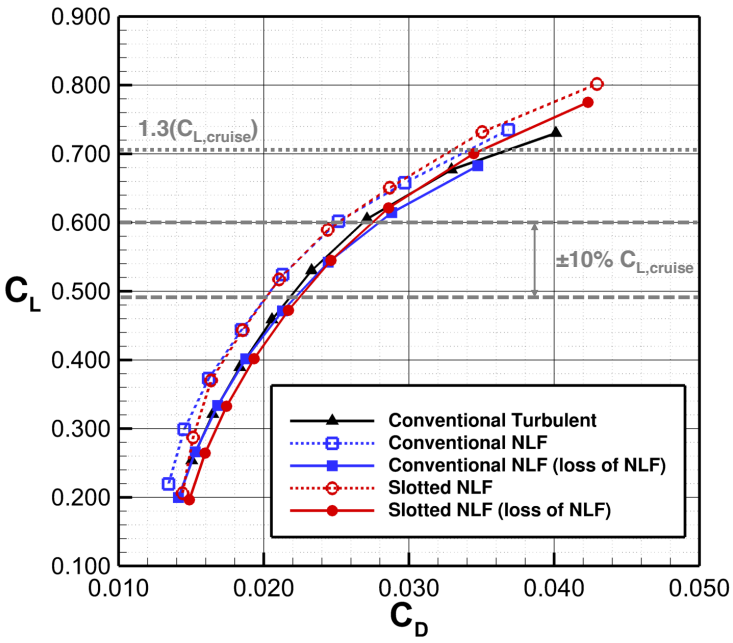

Figure 12. Near-cruise drag polar for the CRM-M8 conventional and slotted wing designs.

Figure 13 shows the sensitivity of the laminar transition fronts due to angle of attack for both the conventional and slotted NLF wing designs. It is observed that as angle of attack is increased beyond the cruise condition (α = 2.1°, C_L = 0.543), the transition front over the inboard wing section moves forward. This is due to an increase in leading-edge acceleration at higher angles of attack, which leads to early transition due to CF growth. In the case of the slotted wing design, this transition front shows greater sensitivity due to pressure peaks that develop over the inboard wing section due to the twist and geometry constraints that are needed to smoothly blend the wing surface over the different airfoil sections. For both designs, laminar flow is consistently achieved over the outboard portions of the wing back to the predicted shock location. For the slotted wing design, the flap also shows limited laminar flow sensitivity to angle of attack over the upper surface. While not shown in the transition fronts, similar observations were made for the flap lower surface with laminar flow obtained over 70% of the flap chord.

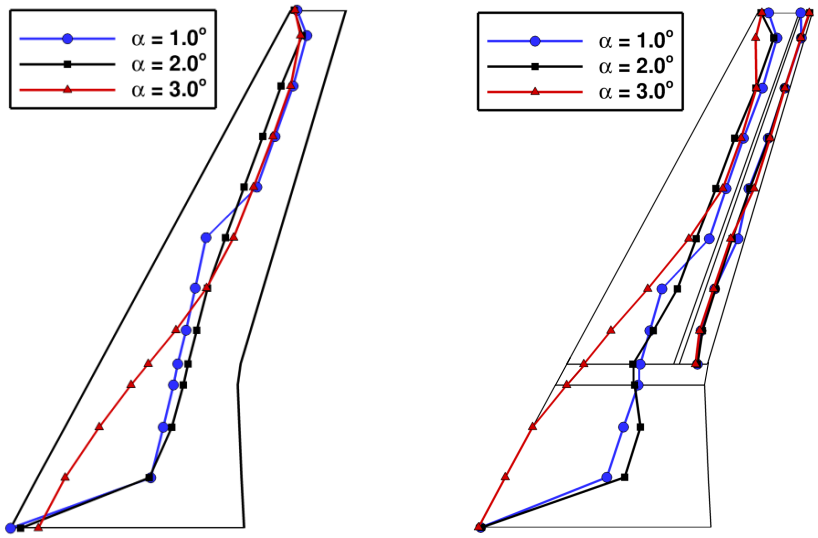

(a) Conventional wing (b) Slotted wing

Figure 13. Transition front sensitivity to angle of attack for conventional (left) and slotted (right) NLF wing variants of the CRM-M8.

Figure 14 provides a comparison of the sectional pressures between the designs at outboard station 8 for α = 2.5° ($C_L \approx 0.6$) and α = 3.5° ($C_L \approx 0.73$). These angles of attack are beyond the cruise angle of attack (α = 2.1°) and highlight the differences in the sectional loading distribution, as well as the shock location and strength. At the upper limit of the near-cruise range, α = 2.5°, similar pressure features are observed between the designs, as seen at cruise. The slotted NLF wing is able to maintain a subsonic flow over the flap upper surface with increased aft loading and a 5% more aft shock location compared to the conventional wing designs. As a result, the load contribution over the forward main element is reduced, and peak upper surface velocities are lower with the slotted wing. As angle of attack is increased to α = 3.5°, beyond the buffet criteria, there is a notable increase in the upper surface shock strength. Both the conventional NLF and slotted NLF wing designs have a shock positioned approximately 10% further aft compared to the conventional turbulent wing. This result can be attributed to reshaping the wing upper surface to achieve a more favorable rooftop gradient at cruise, which delays the forward translation of the shock with increases in angle of attack. Aft of the terminating shock, the conventional wing designs experiences shock-induced boundary layer separation over the upper surface as implied by the linear pressure gradient back toward the TE. The conventional NLF wing shows brief separation following the shock due to the abrupt adverse pressure gradient and a slight recovery to attached flow conditions near the TE. In contrast to the conventional wing designs, the slotted NLF wing demonstrates an ability to maintain attached flow over the flap due to the "dumping velocity" effect of the slot. By maintaining attached flow near buffet conditions, the slotted wing reduces pressure drag due to separation compared to conventional wing designs.

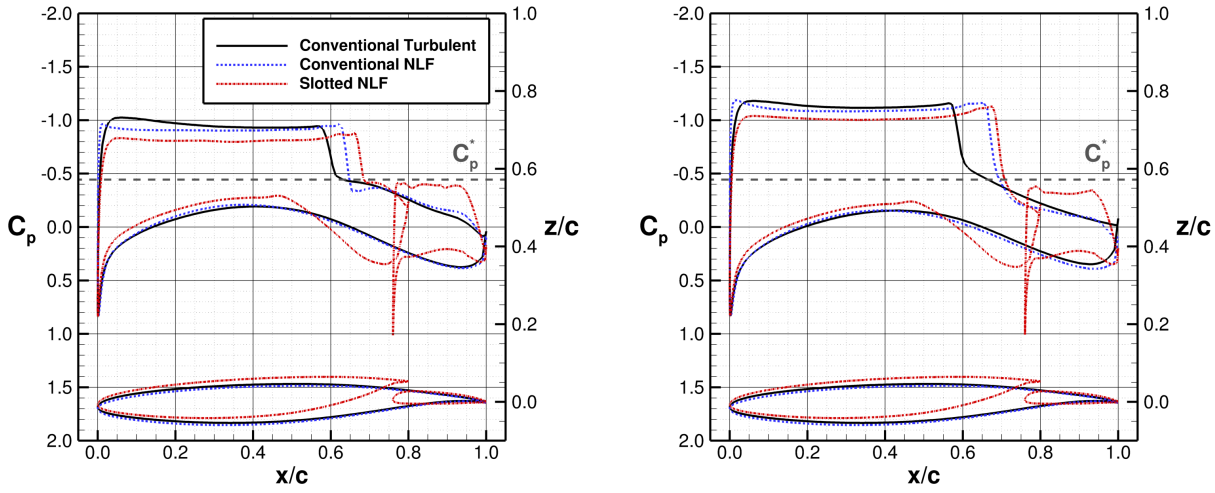

(a) $\alpha = 2.5°$ ($C_L \approx 0.6$)

(b) $\alpha = 3.5°$ ($C_L \approx 0.73$)

Figure 14. Sectional pressures and geometry at outboard station 8 at $\alpha = 2.5°$ and $3.5°$ for the CRM-M8 conventional and slotted wing designs.

B. Drag Rise

In addition to the drag polar, drag rise simulations were conducted for the wing designs over a Mach number range of 0.75 to 0.85 with a Mach number increment of 0.01. At each Mach number, the angle of attack is iteratively changed to converge to the cruise lift coefficient within a tolerance of $\Delta C_L = \pm 0.0001$. This Mach number range includes the constant drag region prior to reaching the critical Mach number, the near-cruise laminar drag bucket, and the transonic drag rise region. Similar to the drag polar simulations, transition predictions were computed using the fully turbulent results to approximate the laminar transition fronts as a function of Mach number. A series of drag rise predictions using USM3D-ME forced laminarization simulations were iteratively run to converge the transition front predictions and estimate the NLF wing performance through the noted Mach number range.

Figure 15 shows the resulting drag rise predictions for each of the three wing designs. Over the low Mach number range, both the conventional and slotted NLF wing designs show a mild drag benefit relative to the conventional turbulent wing design. As Mach number increases to near-cruise conditions, this drag benefit increases as significant skin-friction drag reductions are achieved by reshaping the wings to support large extents of laminar flow. As Mach number is further increased beyond M = 0.82, there is a significant increase in drag due to the strengthening of shocks over the upper surface that lead to flow separation. However, it is observed that the transonic dragrise is attenuated for the slotted wing compared to the conventional wing designs. The slotted NLF wing provides a 20% improvement in L/D at the peak Mach number of 0.85 compared to the conventional turbulent wing and a 9% improvement relative to the conventional NLF wing. At fully turbulent, off-design conditions, the slotted wing matches the performance of the conventional NLF wing with a 10% drag reduction relative to the conventional turbulent wing.

Figure 16 shows the sensitivity of the laminar transition fronts due to Mach number for both the conventional and slotted NLF wing designs. The conventional NLF wing shows limited transition front sensitivity to Mach number with laminar flow achieved back to the upper surface shock over the entire range. In the case of the slotted wing, similar extents of laminar flow are achieved over the wing upper surface with the exception of just near the planform break, for which the use of geometry smoothing constraints led to sensitive pressure peaks near the LE. Over the outboard slotted wing section, laminar flow over the flap upper surface is generally maintained with the exception of the slot flow near Mach 0.83, which introduces a terminating shock near the slot exit and leads to early transition. At Mach 0.85, supersonic flow is maintained aft of the slot before terminating mid flap chord, which leads to a greater extent of laminar flow compared to Mach 0.83. Similar to the drag polar results, it is observed that laminar flow is maintained over a wide range of Mach numbers for both designs.

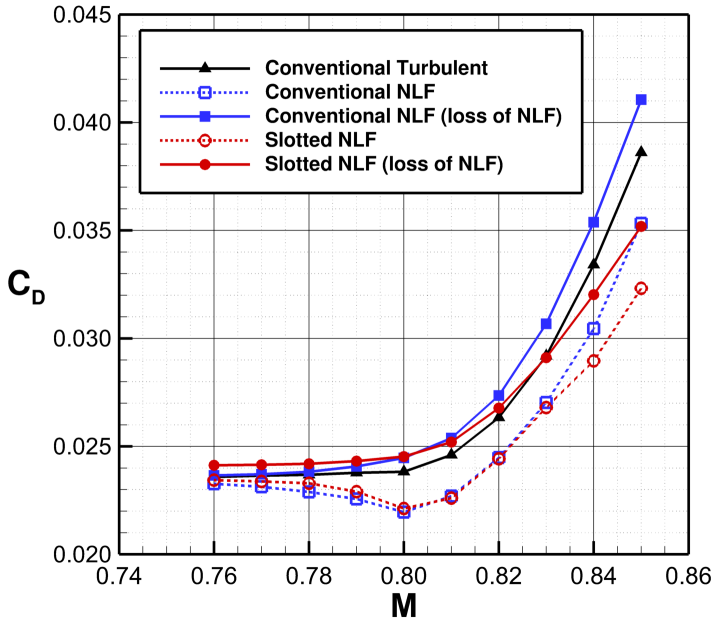

Figure 15. Near-cruise drag rise for the CRM-M8 conventional and slotted wing designs.

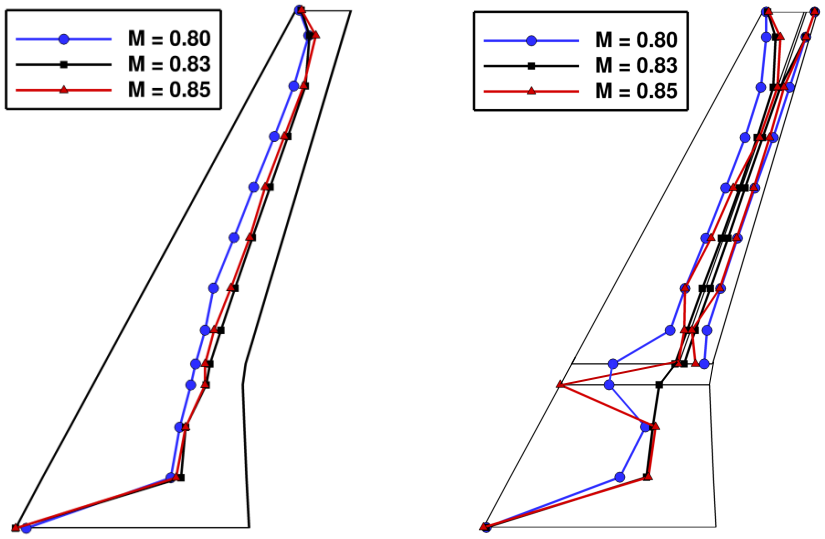

(a) Conventional wing (b) Slotted wing

Figure 16. Transition front sensitivity to Mach number for conventional (left) and slotted (right) NLF wing variants of the CRM-M8.

Figure 17 shows a comparison of the sectional pressures between the designs at outboard station 8 for Mach 0.83 and 0.85. These points fall within the transonic drag rise region and illustrate the growth in upper shock strength with increases in Mach number. At M = 0.83, the conventional NLF and slotted NLF wing designs show an extended favorable pressure gradient over the upper surface with a terminating shock located approximately 10% further aft than the conventional turbulent wing. Similar to the drag polar observations, the conventional turbulent wing shows abrupt shock-induced separation near x/c = 0.7. The conventional NLF wing provides a greater extent of attached flow due to the shift in shock position, but also results in flow separation and mild reattachment toward the TE. In constrast, the slotted NLF wing is able to achieve attached flow over the entire wing due to the beneficial slot "dumping velocity", which promotes a more gradual pressure recovery over the flap upper surface. As Mach number increases to M = 0.85, similar observations can be made with the slotted wing providing attached flow over approximately 95% of the wing upper surface. This observation further illustrates the benefits of the slotted wing at off-design conditions compared to conventional turbulent and NLF wings due to the mitigation of shock-induced boundary layer separation.

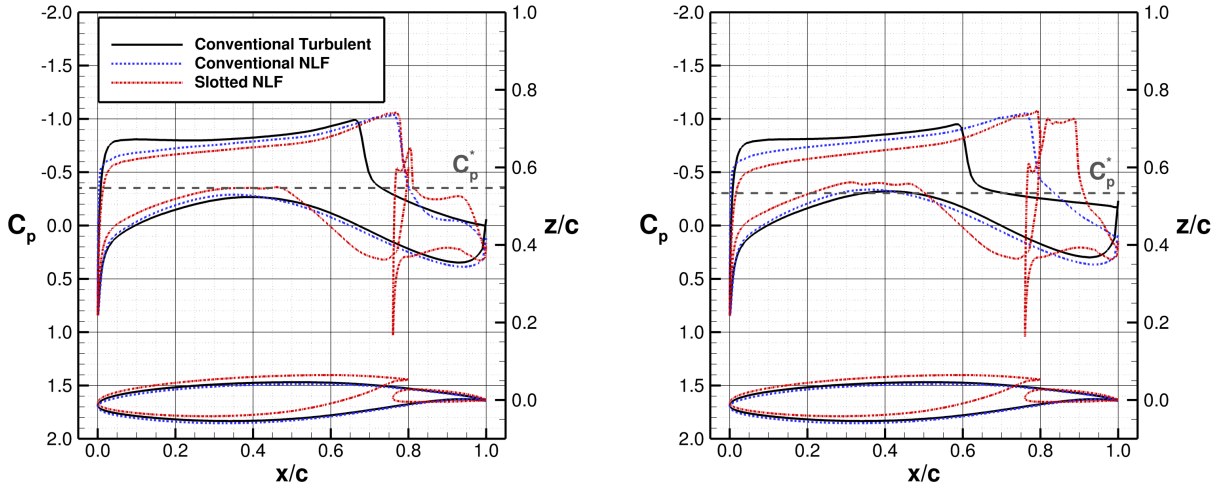

(a) M = 0.83

(b) M = 0.85

Figure 17. Sectional pressures and geometry at outboard station 8 at Mach 0.83 and 0.85 for the CRM-M8 conventional and slotted wing designs.

V. Concluding Remarks

The presented study investigated the aerodynamic performance benefits of a cruise slotted wing with natural laminar flow for transonic transport aircraft. This multielement wing concept includes an intermediate slot, which serves to redirect accelerated airflow from the lower surface of the forward main element toward the upper surface of the flap element. In doing so, this enables the flow along the upper surface of the wing to withstand a more abrupt pressure recovery without separation compared to conventional wings. As a result, the cruise slotted wing can achieve greater aft loading for the potential benefit of reduced shock strength and pressure drag at cruise and off-design conditions. However, a skin-friction drag penalty has been historically recognized as a detriment toward the adoption of the cruise slotted wing technology on next-generation aircraft. A key observation in previous work by the authors showed that this drag penalty could be attributed to the formation of a new boundary layer on the flap, which has a relatively low chordwise Reynolds number and thus, higher skin-friction drag over the aft chord region compared to a supercritical wing. To mitigate this penalty, design techniques for NLF airfoils were leveraged to reshape the cruise slotted airfoil to achieve significant laminar flow extents over the main element upper surface and both surfaces of the flap. The objective was to quantify whether a cruise slotted wing with natural laminar flow could provide these reductions in pressure and viscous drag for single-aisle, transonic transport aircraft.

A knowledge-based aerodynamic design method, CDISC, was coupled to the NASA USM3D-ME flow solver to facilitate the design and analysis of a partial-span, cruise slotted wing with natural laminar flow for a Mach-0.8 variant

of the Common Research Model. Two conventional wing designs, one fully turbulent and one with NLF on the upper wing surface, were also designed using CDISC to provide performance comparisons with modern transport wings at cruise and near-cruise, off-design conditions. At a cruise condition of M_∞ = 0.8, Re_{cref} = 21.1 million, and C_L = 0.543, the slotted NLF wing design showed an 18.4 drag count reduction relative to the conventional turbulent wing and an additional 1.4 drag count reduction compared to the conventional NLF wing. This could be attributed to an 8% increase in total NLF wing area for the slotted wing design compared to a conventional NLF wing due to laminarization of the aft flap and extended regions of laminar flow along the wing upper surface due to a 10% aft translation of the terminating shock position. A near-cruise drag polar also showed that the slotted wing was able to decrease shock-induced boundary layer separation as angle of attack increased compared to conventional wings. At the buffet condition ($1.3*C_{L,cruise}$), the slotted NLF wing showed a 15% improvement in aerodynamic efficiency (L/D) compared to the conventional turbulent wing and a 5% improvement compared to the conventional NLF wing. This reduction in shock-induced boundary layer separation was also observed for a near-cruise drag rise analysis, for which the slotted NLF wing provided a 20% improvement in L/D at the peak dragrise Mach number of 0.85 compared to the conventional turbulent wing and a 9% improvement compared to the conventional NLF wing. Furthermore, transition sensitivity analyses showed that the slotted NLF wing was resilient to changes in angle of attack and Mach number with the exception of the flap, which showed a decrease in laminar flow extents at high Mach numbers due to supersonic flow through the slot that led to early transition.

The results of this study successfully demonstrated the drag-saving benefits of pairing the cruise slotted wing architecture with natural laminar flow design principles for a single-aisle, transonic transport aircraft at cruise and near-cruise, off-design conditions. It is important to note that the current research was limited to a technology assessment using a simplified wing-body configuration and further research is required to assess the drag benefit in consideration of trim drag and propulsor effects. Additionally, no slot brackets were modeled, which could limit the extents of laminar flow achieved on the aft flap element. However, this research only considered a partial-span, cruise slotted wing and additional drag savings may be achieved for a full-span design. Overall, the performance assessment for cruise slotted NLF wings was encouraging and future work is proposed for alternative configurations and/or speed regimes for further evaluations.

Acknowledgments

The authors would like to acknowledge several key researchers and managers at the NASA Langley Research Center who have contributed to the development of Cruise Slotted Wing Technology, including Richard Wahls, William Milholen, Sally Viken, Steve Krist, and Taylor Kate Boyett. This research is funded by the Advanced Air Transport Technology Project within the Advanced Air Vehicles Program. Resources supporting the computational results in this paper were provided by the NASA High-End Computing Program through the NASA Advanced Supercomputing (NAS) Division.

References

[1] Hiller, B., Campbell, R., Lynde, M. N., and Boyett, T. K., "Design Exploration of a Transonic Cruise Slotted Airfoil," AIAA Paper 2021-2525, June 2021. https://doi.org/10.2514/6.2021-2525.

[2] Hiller, B., Campbell, R., and Banchy, M. N., "Transonic Cruise Slotted Wing Design for Commercial Transport Aircraft using CDISC," AIAA Paper 2024-0677, January 2024. https://doi.org/10.2514/6.2024-0677.

[3] Campbell, R., Banchy, M. N., and Hiller, B., "History and Status of the CDISC Aerodynamic Design Method," AIAA Paper 2024-0674, January 2024. https://doi.org/10.2514/6.2024-0674.

[4] Pandya, M. J., Jespersen, D. C., Diskin, B., Thomas, J. L., and Frink, N. T., "Efficiency of Mixed-Element USM3D for Benchmark Three-Dimensional Flows," *AIAA Journal*, Vol. 59, No. 8, 2021, pp. 2997–3011.

[5] Wie, Y.-S., "BLSTA: A Boundary Layer Code for Stability Analysis," NASA/CR-1992-4481, December 1992.

[6] Chang, C.-L., "The Langley Stability and Transition Analysis Codes (LASTRAC): LST, Linear & Nonlinear PSE for 2D, Axisymmetric, and Infinite Swept Wing Boundary Layers," AIAA Paper 2003-974, January 2003. https://doi.org/10.2514/6.2003-974.